Molecular dynamics simulation of heat pulse propagation in single-wall carbon nanotubes

Mohamed A. Osman
School of Electrical Engineering and Computer Science, Washington State University, Pullman, Washington 99164-2752, USA

Deepak Srivastava
NASA Ames Center for Nanotechnology and UARC/UCSC, MS 229-1, Moffett Field, California 94035-1000, USA
(Received 13 January 2005; published 9 September 2005)

The propagation of heat pulses in single-wall carbon nanotubes has been investigated using molecular dynamics simulations. It is found that heat pulses of picosecond duration in (10,0), (7,0), and (5,5) single-wall carbon nanotubes induce several wave packets that propagate at different propagation speeds. The leading wave packets move at the speed of sound corresponding to that of longitudinal acoustic (LA) phonons, followed by wave packets with speeds corresponding to twisted phonon mode (TW), second sound wave, and diffusive components. The waves corresponding to ballistic LA and TW phonon modes in (10,0) and (7,0) zig-zag nanotubes carry more heat energy than in (5,5) armchair nanotubes. The energy carried by wave packets corresponding to the speed of second sound waves is larger than those carried by TW and LA modes. These are used to explain the higher thermal conductivity of zig-zag nanotubes as compared to armchair nanotubes reported recently.

DOI: 10.1103/PhysRevB.72.125413 PACS number(s): 66.70.+f, 65.80.+n, 65.40.−b, 63.20.Kr

I. INTRODUCTION

The high thermal conductivity of carbon nanotubes (CNTs) has attracted a lot of attention recently because of its potential applications in thermal management. For example, it is well known that heat dissipation is one of the major issues facing ultra large scale integration (ULSI) technology. Additionally, during the re-entry phase, the space shuttle is subjected to intense heat and special materials are required to absorb and dissipate the heat generated from the exposed surface area. The development and optimization of the thermal properties of the heat pads and packages using materials like CNTs, which has large thermal conductivity, requires the understanding of both the transient and steady state heat flow rates. The steady state heat flow represented by thermal conductivity has been recently studied vigorously using both experimental and theory/simulation based approaches.[1–10] The measured thermal conductivities of single-wall and multiwall carbon nanotubes exhibit a monotonic increase up to room temperature.[1–3] This is in contrast to the thermal conductivities of diamond and graphite which exhibit the typical temperature dependence of nonmetallic crystals[6] and reach their maximum values well below room temperature (175 K for diamond and 100 K for graphite).[4–6] The measured thermal conductivity of multiwall nanotubes (MWNT) reaches a maximum above room temperature and its value at 300 K is significantly higher than those reported for diamond and graphite at 300 K.[4,5] The reported experimental values for single-wall carbon nanotubes (SWCNT) are smaller because bundles or ropes of SWCNT were used in the measurements.

The fact that anharmonic phonon interactions (Umklapp processes) and defects are responsible for the drop in the thermal conductivity at high temperatures, indicates different phonon processes in carbon nanotubes compared to diamond and graphite. Whereas a nanotube can be viewed as a rolled up graphene sheet, there is no one to one correspondence between the acoustic phonon modes in graphite and nanotubes. The acoustic phonon modes in SWNT include (1) doubly degenerate transverse acoustic modes (TA) that involve vibrations perpendicular to the nanotube axis (as in plucking a string), (2) longitudinal acoustic mode (LA) with vibrations along the nanotube axis, and (3) twisting mode (TW) with displacements in the cylindrical plane perpendicular to the axis of an isolated nanotube. The out of plane tangential acoustic (TA) mode in graphene sheet corresponds to the radial breathing mode in a nanotube (TB). However, the radial breathing mode has nonzero frequency at $k=0$ and thus can be viewed as an optical phonon mode. Changes in nanotube diameters can excite different radial phonon modes that participate in transmitting heat and phonon-phonon interactions at high temperatures. Recent theoretical investigation of relaxation through Umklapp processes in zig-zag nanotubes have shown phonon mean free path length of the order of 1 μm at 300 K.[11] The one-dimensional nature of the carbon nanotubes makes boundary scattering very important. The electron concentration in the semiconducting zig-zag nanotubes (10,0) and (7,0) with energy gaps of 0.45 eV and 0.65 eV, respectively, varies as $\exp[-E_g/2k_BT]$ where k_B is the Boltzmann constant, T is the temperature, and the energy gap $E_g=2.5\pi/\sqrt{3(m^2+n^2+mn)}$ eV for (m,n) semiconducting nanotubes.[21] Consequently, the electron concentration is negligible at very low temperatures. This results in negligible electron contribution to the heat capacity C and the thermal conductivity $\kappa=\frac{1}{3}\lambda\nu_sC$, where λ is the phonon mean free path length and ν_s is the speed of sound for phonon contribution. For electronic contribution one uses the electron mean free path length and the Fermi velocity. The estimation of the ratio of the electron contribution to phonon contribution to the heat capacity in the metallic nanotubes such (10,10) armchair nanotubes, ranges from negligible over all temperature range in Ref. 7 to decreasing from 100% to below 20% as temperature changes from 0 K to 200 K.[12] However, the ratio of the thermal conductance κ_{el}/κ_{ph} based

on the theoretical model in Ref. 12 is an order of magnitude higher than the experimentally observed ratio.[2,3] Phonon contribution is stronger in (10,10) nanotube compared to (5,5) nanotube at low temperatures because of the lower optical phonon energy gap which varies as $1/R^2$, where R is the radius of the nanotube.[12] However, in both cases the acoustic phonons are active below the optical phonon energy gap and electron concentration is the same in (5,5) and (10,10) because both are metallic. Therefore, we assume that the above conclusion regarding the κ_{el}/κ_{ph} ratios also holds in (5,5) SWNT. The direct simulations using molecular dynamic (MD) approach, which includes the underlying phonon-phonon interactions in a natural way, are ideal platform for investigating thermal conductivity and the processes involved in transient heat transport. This approach does not take into account any electron contributions which we assume to have negligible effects based on the above arguments.

In a recent investigation using molecular dynamics simulations, we have reported that the thermal conductivity of (10,0) zig-zag single-wall carbon nanotube was higher than that of (5,5) armchair nanotube especially at low temperature ($T=100$ K).[8] The diameter of the (10,0) nanotube is 16% larger than that of the (5,5) nanotube. This raises the question about the nature of energy transport processes in each nanotube and whether these processes are affected by chirality or the diameter of the nanotube. For example, excitation of different phonon modes may be responsible for the earlier reported difference in the thermal conductivities of zig-zag and armchair nanotubes.[8,11] The Fourier approximation used in steady state thermal conductivity calculations, however, does not provide any information about the participating phonon modes and the energy carried by each phonon mode.

The application of strong heat pulses, on the other hand, generates several waves propagating at different speeds corresponding to different phonon modes, can provide information about individual modes and their contribution towards the overall heat transport.[13–15] Heat pulse measurements in NaF at low temperatures revealed Ballistic LA and TA phonon mode propagation as well as second sound waves at temperatures below 14 K.[14] Therefore, heat pulse experiments provide quantitative information on transport by diffusion, ballistic phonons, and second sound waves. The speeds of the leading edges of pulses arriving at the detector are determined from the arrival times and the sample length and used to determine the ballistic phonon mode (LA or TA).[14,15] The second sound waves can be observed, as in the experiments reported in Ref. 14, when the momentum conserving normal phonon scattering processes are dominant compared to the momentum randomizing Umklapp phonon scattering processes. The high thermal conductivity in carbon nanotubes and its increase up to room temperature has been attributed to the long phonon mean free path length.[1–3] As Umklapp processes mainly determine the mean free path length, it is also feasible to assume that normal phonon-phonon scattering processes (N-processes) dominate up to room temperature or at least over a wider range of temperatures compared to that in NaF. Consequently, one can expect second sound waves to be observed in nanotubes. In heat pulse propagation experiments, the known speeds of phonon modes in the material under investigation are used to distinguish between different phonon modes. Consequently, heat pulse simulations can provide insight into how heat flow occurs in nanotubes, the important contributing phonon modes, and their dependence on the nanotube chirality and diameter.

In this paper we present a study of the thermal energy transport in single-wall carbon nanotubes subjected to intense heat pulses. Earlier molecular dynamic studies on pulsed heat propagation in alpha iron demonstrated energy flow by LA and TA modes and second sound waves.[13] Low temperatures and pure crystalline materials are required to observe second sound waves that are not attenuated by dissipative scattering processes. The molecular dynamics (MD) simulations thus provide an ideal platform for investigating these properties by controlling the temperature of the CNT, shape and duration of heat pulses assuming the perfect crystalline structure. We have used molecular dynamic simulations to examine transient heat pulse propagation in (7,0), (10,0), and (5,5) single-wall carbon nanotubes with particular emphasis on the role of nanotube chirality and diameter. The heat pulse is found to generate wave packets that move at speed of sound corresponding to different phonon modes, second sound waves, and diffusive components. The relative amount of heat energy carried by waves corresponding to ballistic LA, TW phonon modes and second sound in zig-zag and armchair nanotubes are also investigated.

II. SIMULATION APPROACH

The MD simulations use the Tersoff-Brenner bond-order potential and solve Hamilton's classical equations of motion with predictor-corrector algorithm with fixed time step of 0.5 femtosecond (fs).[16,17] In order to examine heat pulse propagation in (10,0), (7,0), and (5,5) nanotubes, each nanotube is divided into 250 slabs. The width of each slab was equal to 4.26 Å for (10,0) and (7,0) nanotubes and 4.92 Å for (5,5) nanotube. For the simulations reported here, the number of atoms per slab is 40 atoms in (10,0) and (5,5) nanotubes and 28 atoms in (7,0) nanotube. The number of atoms per slab increases as the diameter of the nanotube increases. The axis of the tube was aligned along the z-axis with the free end of the nanotube at $z=0$, while the far end of the nanotube was held rigid. In order to apply heat pulse and ensure smooth temperature transition from the boundary to the region of interest on the nanotube, the boundary region was chosen to extend over five slabs.[18]

A strong heat pulse of one picosecond (ps) duration, and 0.05 ps rise and fall times was applied to the left boundary region. During the rise time of the heat pulse, the temperature of the five slabs near the left boundary was ramped up gradually to a final temperature $T_f=800$ K, assuming a linear increase in temperature, held constant at 800 K for an other 0.9 ps, and then decreased to a final temperature of 0.01 K. The temperatures in the slabs are maintained at the desired temperature T_f by scaling the velocities of each atom i in the slabs at the beginning of each time step from an initial value of v_i to final v_i' according to $v_i'=v_i\sqrt{T_f/T_i}$, where T_i is the current slab temperature before scaling. This amounts to add-

ing (or subtracting) energy $\Delta E = \Delta E_{\text{kin}}$ to the boundary slabs

$$\Delta E = \sum_{i=1}^{N_L} \frac{1}{2} m_i (v_i'^2 - v_i^2), \tag{1}$$

where N_L is the total number of atoms in the five boundary slabs and m_i is the mass of atom i (taken to be carbon atom). The temperature T is defined as $\frac{1}{2}mv_i^2 = \frac{3}{2}k_B T$ which we also refer to as the kinetic temperature to emphasize the fact that it is used as a measure of the kinetic energy. During each simulation time step the boundary atoms (i.e., atoms in the five boundary slabs) interact with interior atoms resulting in energy exchange and heating of the interior atoms. The amount of energy added at each time step to atoms in the five boundary slabs will depend on how much energy was exchanged between the boundary atoms and the interior atoms. A reflecting boundary condition is imposed at the left boundary which amounts to reversing the sign of the z-component of the velocity vector of atoms approaching the boundary. These events are minimized by setting the slab boundary midway between bonded atoms (i.e., no atoms are at the boundary). During the 0.05 ps fall time, the temperature of the boundary slabs was decreased at the same rate in all slabs to reach a final temperature of 0.01 K. This amounts to removing energy from boundary slab atoms during fall time. The temperature of the boundary slabs was held at 0.01 K for the remainder of the simulation and only heat energy transferred to the interior of the nanotube contributes to pulse propagation. Because all nanotubes were subjected to identical heat pulse conditions, the amount of heat energy that is transferred to the interior of the nanotubes is determined only by the efficiency of the interactions between the atoms in the boundary and interior slabs. For the simulations reported in this paper, the net energy added to the (10,0), (5,5), and (7,0) nanotubes were 56.2 eV, 49.42 eV, and 37.13 eV, respectively. The number of atoms in the boundary slab layers were 200 atoms for the (10,0) and (5,5) nanotubes and 140 atoms for the (7,0) nanotube. The net energy added per atom in the boundary slabs, which provides a more accurate comparison between the different nanotubes, can be shown to be 0.281 eV, 0.247 eV, and 0.265 eV for the (10,0), (5,5), and (7,0) nanotubes, respectively.

The temperature of each slab was spatially averaged over five slabs centered at the slab of interest. The minimum time scale τ_m for time averaging is taken to be the time required for a ballistic LA mode to traverse a single slab which corresponds to about 25 fs for a (5,5) nanotube which is significantly larger that the time step of 0.5 fs used in the simulations. In our simulations, the temperature was time averaged over 200 time steps which corresponds to 100 fs. The boundary at the far end of the nanotube also consisted of several slabs with the outermost slab rigidly held in place. The remaining slabs were held in equilibrium at the simulation temperature by applying a Gaussian random force, satisfying fluctuation-dissipation theorem, which ensured that no reflection from the boundary to the oncoming propagating waves occurs. The one dimensional nature of the nanotube simplifies boundary conditions, as one does not have to worry about the scattering in the transverse directions. The atom's motion and configurations in the transverse or radial directions are governed by the intrinsic forces that maintain the shape of the nanotube.

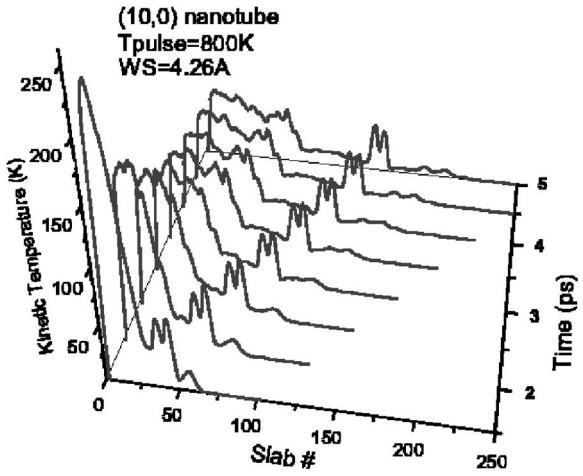

FIG. 1. Temporal and spatial distribution of kinetic temperature along the (10,0) SWNT.

The MD simulations of single-wall carbon nanotubes start by quenching the system to 0 K for 2000 time steps which was long enough to ensure convergence of the total potential energy (smaller than 10^{-6} eV change). This was followed by an other run for 2000 time steps to achieve thermal equilibrium at 0.01 K before the application of strong heat pulse of one picosecond duration, as described earlier. The simulation was stopped before the leading waves reached the right boundary, even though the boundary slabs and conditions would have ensured no reflection back into the system. The instantaneous temperature distribution along the nanotube were calculated at each time step and recorded every 200 time steps in addition to the time and spatially averaged temperatures. In order to determine the propagation speeds of the leading waves, the slab numbers corresponding to the peak locations at given time intervals are recorded. The speed is then determined from the spatial distance traversed by the particular wave during a given time interval. The average speed for each peak was determined from linear fit of the peak locations versus time.

III. RESULTS AND DISCUSSION

An example of the temporal and spatial variation of the kinetic temperature in (10,0) nanotube obtained from the MD simulations is shown in Fig. 1. The heat pulse induces clearly defined wave packets that propagate on the nanotube. The leading wave packets move at higher speeds as compared to the diffusive background. The shapes of wave packets P2 and P3, as shown in Fig. 2, change and the peak intensity of P2 decreases by 15% between 3 ps and 5 ps while that of P3 stays constant during the same period. On the other hand the peak intensity of the weak leading wave packet P1 stays constant and the shape does not change as seen in Fig. 2. The leading wave packets are followed by a dual peak wave packet that undergoes very minor changes in its shape and the peak intensities slowly decay to a final kinetic tempera-

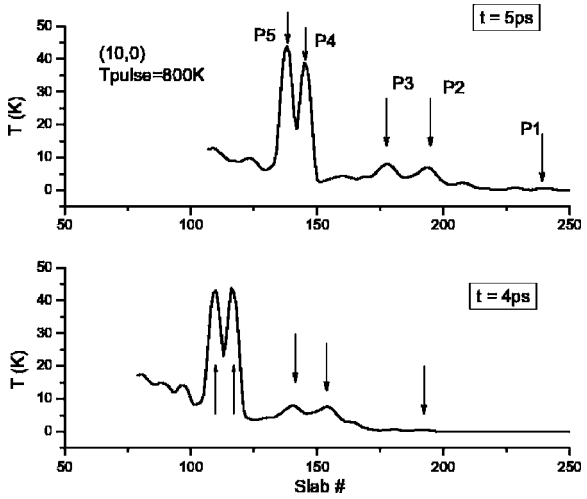

FIG. 2. Spatial distribution of kinetic temperature along the (10,0) SWNT at times 4 and 5 ps after application of the pulse.

ture around 40 K at 5 ps. The time axis for this analysis has been started at 1.5 ps to avoid the initial large transient kinetic temperature values that make it difficult to observe and analyze the low intensity propagating waves from left to right. By shifting the time axis to 1.5 ps, the plotted maximum temperature has been reduced from 400 K to less than 100 K, which allows for better resolution of the wave packets with smaller peaks. The distance along the nanotube axis has been normalized by the slab width and is plotted as slab numbers.

The three-dimensional view in Fig. 1 provides a clear picture of how waves develop and propagate as separate wave packets on the nanotube. The details of the low amplitude higher speed wave packets are not clearly seen in the figure because of the slow moving large diffusive components. Figure 2 shows the details of the frontal leading waves leaving out the diffusive part of temperature distributions at times 4 and 5 ps. For detailed description and analysis, we focus on how peaks P1 and P2 in Fig. 2 propagate. Following the procedure described in Sec. II, the average speed of peaks P1 and P2 were found to be 20.6 km/s and 16.6 km/s, respectively. These speeds are very close to the speed of sound associated with longitudinal acoustic (LA) and twisted phonon modes (TW), respectively.[19] The values obtained from the MD simulations are similar to the theoretically calculated sound velocities of LA and TW phonons, in (10,10) armchair nanotubes, which were reported to be 20.35 km/s and 15 km/s, respectively.[19] The shape of the leading wave packet (identified as arising from LA mode) did not change and had a peak kinetic temperature of 0.6 K and a full-width at half maximum of 2.4 nm as shown in Fig. 3. The centers of the three peaks in Fig. 3 have been shifted to coincide with each other to compare the number of slabs over which the peaks of the LA mode for the different nanotubes are spread. The slab number for the x-axis does not reflect the actual location of the peak along the nanotube, however, it allows comparison of the width of each peak. The wave packet P2, corresponding to the TW mode, has higher peak energy and undergoes a fast decay from an initial value of 17 K to 7.0 K at 5 ps as shown in Fig. 4(a). The temperature data in Fig. 4(a) for (10,0) nanotube can be fit to $T = 6.6 + 47.9e^{-t/1.06}$ K over the time range 1.6–5.0 ps and yields a decay time constant of 1.06 ps. For comparison, the

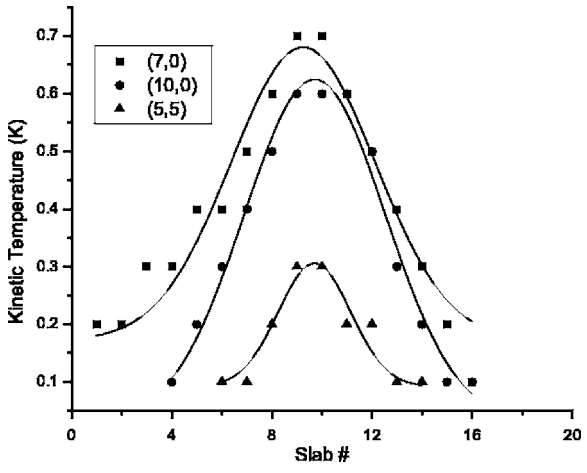

FIG. 3. Shape of the leading LA mode in (10,0), (7,0), and (5,5) nanotubes at time=4 ps. The peaks are shifted to have all of them centered at slab 10. The line through the data points represents the best Gaussian fit.

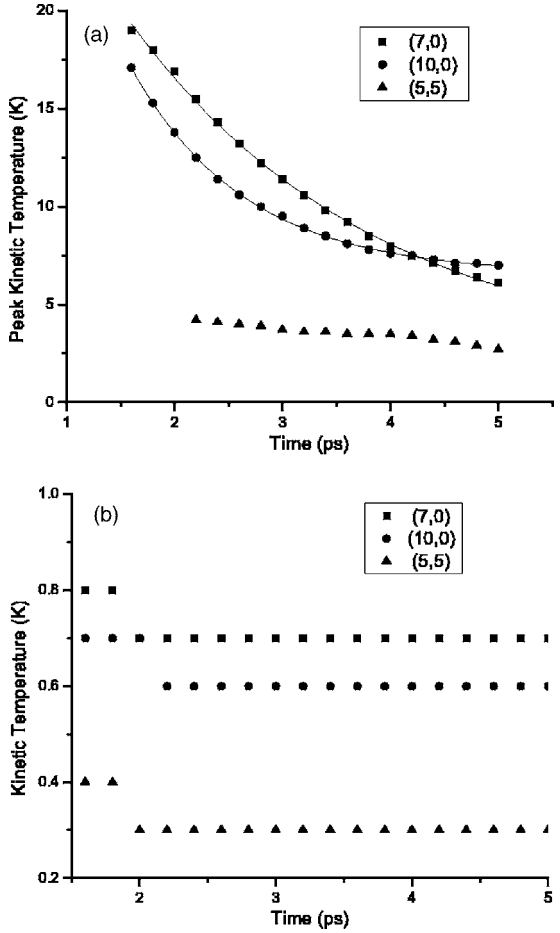

FIG. 4. Time dependence of the peak kinetic temperature of (a) TW mode wave packets (the line represents the best exponential decay fit), (b) LA mode wave packets.

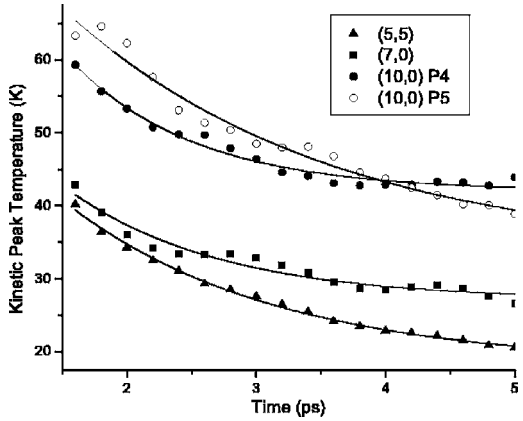

FIG. 5. Time dependence of the peak kinetic temperature of the second sound waves. The lines through data points represent best exponential decay fit.

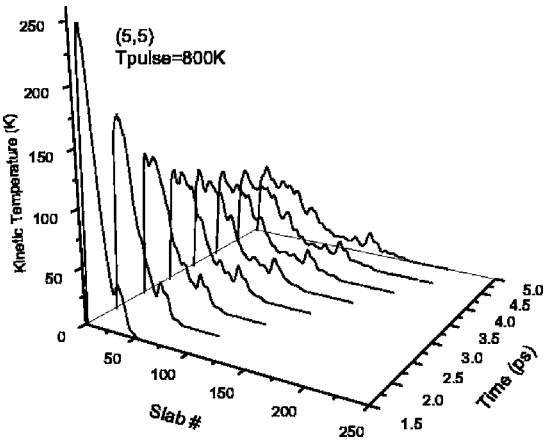

FIG. 6. Temporal and spatial distribution of kinetic temperature along the (5,5) SWNT.

time dependence of the peak temperature for peak P1 is shown in Fig. 4(b). At 5 ps after the onset of the pulse, wave packet P2 had a much higher peak kinetic temperature of 7 K and a width at half maximum of 4.3 nm. Therefore the atomic motions within the TW wave packet P2 carry about 20 times higher overall kinetic energy as compared to the atomic motions within the P1 wave packet.

The strongest wave packets in Fig. 2 are P4 and P5 and they propagate together at a speed of 12.2 km/s. Later we show that this speed corresponds to that of second sound waves that have been generally observed in low temperature thermal propagation in defect free crystalline materials. The temperature data for peaks P4 and P5 in Fig. 5 for (10,0) nanotube can be fit to $T=33.2+69.9e^{-t/2.06}$ K and $T=42.0+90.2e^{-t/0.97}$ K, respectively. This yields decay time constants 2.1 and 1.0 ps for peaks P4 and P5, respectively. At 5 ps after the onset of the pulse, wave packets P4 and P5 had peak temperatures 39.0 K and 44.0 K and full width at half maximum of 1.9 nm and 2.3 nm, respectively. Note that these two wave packets also remain spatially confined as compared to the leading wave packets P1, P2, and P3. Furthermore, the total energy in the wave packets P4 and P5, as computed from the area of the curve under the Gaussian fit, is three times larger than the combined P2 and P3 wave packets. Consequently, one can conclude that the leading wave packets in zig-zag (10,0) nanotubes propagate at the sound velocities of LA and TW modes. However, the largest amount energy is carried by wave packets propagating at 12.2 km/s, which we later identify and explain as second sound waves.

The MD simulations were repeated for (5,5) armchair nanotube. The nanotube consisted of 250 slabs, each 4.92 Å wide. The heat pulse shape and duration was identical to the one used in (10,0) nanotube. The temporal and spatial variation of the kinetic temperature in (5,5) nanotube is shown in Fig. 6. The details of the spatial distribution of the temperature along the nanotube after leaving out the diffusive component at 3 and 4 ps are plotted in Fig. 7. The shape of the leading wave packet P1 for the (5,5) nanotube at 4 ps is shown in Fig. 3. The wave packet for the (5,5) nanotube has smaller spatial spread and lower peak kinetic temperature compared to the values for the (10,0) and (7,0) nanotubes. The peak values for the leading wave packets in the (5,5) nanotube also decay slower throughout the simulations. The very weak leading wave packet (P1) propagates at a speed of 20.3 km/s corresponding to the speed of LA phonon mode. The leading wave packet is followed by a relatively broader and stronger peak (P2) moving at 16.7 km/s speed, which is closer to the sound velocity of the twisted phonon (TW) in the (5,5) armchair nanotube. The wave packet P3 results from a decay of wave packet P4 and takes a distinct shape after 4 ps and travels at 17.0 km/s. The stronger P4 wave packet propagates at 12.9 km/s, which we later identify as second sound wave.

The simulation was then repeated for a (7,0) nanotube with the same heat pulse parameters to examine how the change in nanotube diameter will affect energy flow through the nanotube and how phonon modes will propagate. The temporal and spatial variation of the kinetic temperature of (7,0) nanotube is shown in Fig. 8. The energy carried by leading wave in (7,0) nanotube is larger than that of the leading wave packet of the (5,5) nanotube as shown in Fig. 3. Following the procedure described for the (10,0) and (5,5) nanotubes, the propagation speeds were determined and pho-

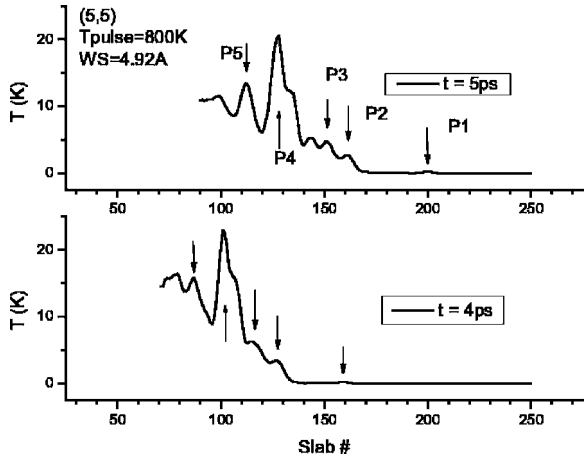

FIG. 7. Spatial distribution of kinetic temperature along the (5,5) SWNT at times 3 and 4 ps after application of the pulse.

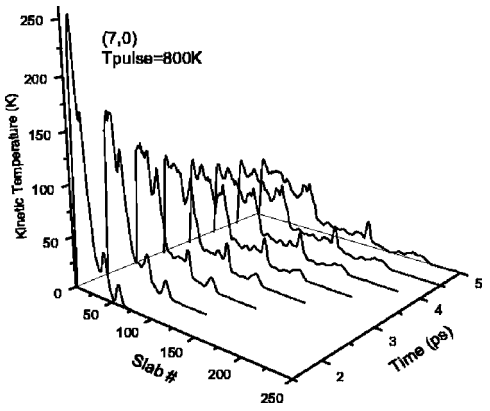

FIG. 8. Temporal and spatial distribution of kinetic temperature along the (7,0) SWNT.

non modes were assigned for propagating wave packets. The energy carried by the TW phonon mode in (7,0) nanotube is comparable to that in (10,0) nanotube and is larger than in (5,5) nanotube based on peak kinetic temperature decay shown in Fig. 4. On the other hand the energy carried by the wave packets P4 and P5, not shown, is found to be smaller than the (10,0) nanotube. For all three nanotubes, the results for the sound speed of the different modes are summarized in Table I.

The above results indicate that both LA and TW phonon modes are excited in response to the application of picosecond heat pulse. Additionally, they also show that the fraction of energy carried by these modes is larger in zig-zag (10,0) and (7,0) nanotubes compared to the armchair (5,5) nanotube. For example, the peak energy of the LA mode in (5,5) SWNT is 50% smaller than in (7,0) SWNT and its width is smaller as can be seen in Fig. 3. For the TW mode, the peak kinetic temperature in (5,5) SWNT is also about 50% smaller than in (7,0) and (10,0) nanotubes. The fact that the energy added to (5,5) nanotube is 12% and 7% smaller than the energy added to (10,0) and (7,0) SWNTs, respectively does not account for the 50% reduction in the energy carried by the LA and TW modes. Furthermore, the TW modes were strongly excited as compared to LA phonon mode in all nanotubes and exhibited a faster decay rates as compared to the decay rates of the weak LA mode.

The wave packets P4 and P5 propagate at speed approximately equal to 12 km/s in all the nanotubes as can be seen from Table I. These wave packets can also be analyzed in comparison with the propagation speed data of known phonon modes. The propagation speed data, as seen in Table II, shows that for TW modes propagation speeds (V_W) vary from 12.0 km/s to 15.0 km/s while for the transverse breathing (TB) phonon modes the speeds (V_B) range from 12.3 km/s to 42.0 km/s.[19–25] This large variation, however, arises from the differences in values of force constants and Young's modulus used in different methods and can overlap with the propagation speed of second sound waves. To examine the possibility of the occurrence of the second sound wave, the ratio R of the speed of wave packet P1 (V_{LA} mode) to the average speed of the wave packets P4 and P5 (V_{S2}), was computed for all three nanotubes. The ratio R was found to be 1.69 in (10,0), 1.68 in (7,0), and 1.62 in (5,5) nanotubes. These ratios deviate from $\sqrt{3}$, by 2%, 3%, and 6% in (10,0), (7,0), and (5,5) nanotubes, respectively. This ratio was used to predict the presence of second sound waves at low temperatures in α-iron and NaF,[13–15] and it is expected to be $\sqrt{3}$ for second sound waves for good crystalline materials. The second sound waves arise when momentum conserving phonon scattering events (N-processes) are far more frequent as compared to momentum destroying collisions as temperature increases in the material. Under such conditions, the energy propagates as "a collective temperature pulse with a characteristic velocity (second sound wave velocity) that is determined by the interaction of different phonon modes in the system."[15] In carbon nanotubes, the momentum destroying Umklapp scattering processes are far less frequent at low temperatures as compared to the N-process and only begin to play a major role above room temperature which is responsible for the monotonic increase in the thermal conductivity of carbon nanotubes up to room temperature.[1–3] The local kinetic temperature within P4 and P5 wave packets are well below room temperature and the nanotube temperature is below 0.1 K which makes N-processes dominant. Furthermore, as can be seen from the three dimensional plots in Figs. 1, 6, and 8 other modes (TW) are generated as the peaks of modes P4 and P5 decrease. This supports the selection that the peaks P4 and P5 represent second sound waves. Further dynamic investigations will be needed and attempted in future with Tersoff-Brenner potential to analyze the dynamics of individual phonon modes and confirm the assignment discussed above. We note, however, that the above assignment of P4 and P5 as second sound wave does not affect in any way the main results and conclusions of this work,

TABLE I. Speeds in km/s of the leading propagating wave packets in (10,0), (7,0), and (5,5) single-wall carbon nanotubes determined from heat pulse simulation.

Peak	(10,0)	(7,0)	(5,5)
P1	20.6 (LA)	21.3 (LA)	20.3 (LA)
P2	16.4 (TW)	18.1 (TW)	16.2 (TW)
P3	15.8 (TW)	16.2 (TW)	17.0 (TW)
P4	12.2	12.7	12.9
P5	12.2	12.6	12.3

TABLE II. Speeds of sound waves associated with longitudinal (V_L), transverse (V_T), twisted (V_{TW}) acoustic, and breathing (V_B) phonon modes in carbon nanotubes.

V_L (km/s)	V_T (km/s)	V_{TW} (km/s)	V_B (km/s)	References
20.35	9.43	15.0		19
21.7		14.0	42.8 km/s	20
20.35	24.0, 9.0	15.0		21
20.7	14.1	14.1		22
19.9		12.3		23 and 24
19.9		12.3	12.3	24
		15.0 (13.0)		25

i.e., in general the non-diffusive energy carried by the modes P1-P5 for zig-zag type nanotubes (7,0) and (10,0) are larger than the energy carried by similar modes in the armchair type (5,5) nanotube.

Assuming that similar propagating modes carry the bulk of thermal energy transport under equilibrium conditions as well, the above comments support the observation that for the same temperature gradient, one can expect higher heat flux in (10,0) zig-zag nanotubes as compared to the (5,5) armchair nanotubes.[8,11] Furthermore, the energy carried by second sound waves in (5,5) SWNT is smaller by more than 50% compared to (10,0) and (7,0) nanotubes. This translates to higher thermal conductivity for the zig-zag nanotubes compared to armchair nanotubes. As the nanotube diameter increases, more modes are excited which also contribute to heat flow. A more detailed analysis of the propagation speeds of the individual phonon modes and simulation of larger diameter nanotubes, in future, will be needed to obtain more quantitative dynamic results.

Lastly, in this section, we note that the dynamics of heat pulse and leading modes propagation through carbon nanotubes, as described and analyzed above, also gives a qualitative view of how different components of thermal transport, i.e., ballistic phonon modes, second sound waves, and diffusive heat, propagate on a pristine carbon nanotube. The speed, nature and energy content of the dominant modes in thermal transport maybe useful in deciding the length of nanotubes and duration of simulations needed to achieve converged values of thermal conductance in this one-dimensional system. Currently, for different nanotubes, there is some variation in the values of the simulated thermal conductivity reported in the literature. The above simulations and the resultant analysis may be useful in explaining the observed variation as a function of tube length and simulation time duration.

IV. SUMMARY

Heat pulse propagation of picosecond duration in armchair (5,5) and zig-zag (10,0), (7,0) single-wall carbon nanotubes has been investigated using MD simulations. It is found that LA, TW phonon modes, and second sound waves are excited and propagate as the leading wave packets. The energy carried of the LA, TW phonon modes, and the second sound waves in the zig-zag type (10,0) and (7,0) nanotubes is higher than the energy carried by similar modes in the (5,5) armchair nanotube. Furthermore, the largest amount of energy is found to be carried by waves moving at the speed of second sound waves. These results are consistent with the recently reported higher steady state thermal conductivity values for the zig-zag carbon SWNT compared with armchair SWNT at low temperatures.[8,11]

ACKNOWLEDGMENTS

We acknowledge partial support from the Center for Digital-Analog Integrated Circuits and AFRL/VSSE. The initial work on this project was started as M.O. was supported through the Educational Associates Program at NASA Ames Research Center. Part of this work D.S. is supported by NASA Contract No. NAS2-03144 to UARC.

[1] P. Kim, L. Shi, A. Majumdar, and P. L. McEuen, Phys. Rev. Lett. **87**, 215502 (2001).
[2] J. Hone, M. Whitney, C. Piskoti, and A. Zettl, Phys. Rev. B **59**, R2514 (1999).
[3] J. Hone, M. C. Llaguno, N. M. Nemes, A. T. Johnson, J. E. Fischer, D. A. Walters, M. J. Casavant, J. Schmidt, and R. E. Smalley, Appl. Phys. Lett. **77**, 666 (2000).
[4] J. E. Graebner *et al.*, Diamond Relat. Mater. **7**, 1589 (1998).
[5] B. T. Kelly, *Physics of Graphite* (Applied Science, Essex, England, 1981), Chap. 4.
[6] R. Berman, *Thermal Conduction in Solids* (Oxford University Press, Oxford, 1976), Chap. 3.
[7] L. X. Benedict, S. G. Louie, and M. L. Cohen, Solid State Commun. **100**, 177 (1996).
[8] M. A. Osman and D. Srivastava, Nanotechnology **12**, 21 (2001).
[9] A. Cummings, M. Osman, D. Srivastava, and M. Menon, Phys. Rev. B **70**, 115405 (2004).
[10] E. González Noya, D. Srivastava, L. A. Chernozatonskii, and M. Menon, Phys. Rev. B **70**, 115416 (2004).
[11] Y. Xiao, X. H. Yan, J. X. Cao, and J. W. Wang, J. Phys.: Condens. Matter **15**, L341 (2003).
[12] T. Yamamoto, S. Watanabe, and K. Watanabe, Phys. Rev. Lett. **92**, 075502 (2004).
[13] R. A. McDonald and D. H. Tsai, Phys. Rep. **46**, 1 (1978).
[14] H. E. Jackson and C. T. Walker, Phys. Rev. B **3**, 1428 (1971).
[15] T. F. McNelly, S. J. Rogers, D. J. Channin, R. J. Rollefson, W. M. Goubau, G. E. Schmidt, J. S. Krumhansl, and R. O. Pohl, Phys. Rev. Lett. **24**, 100 (1970).
[16] J. Tersoff, Phys. Rev. Lett. **61**, 2879 (1988).
[17] D. W. Brenner, Phys. Rev. B **42**, 9458 (1990).
[18] J. X. Cao, X. H. Yan, Y. Xiao, Y. Tang, and J. W. Ding, Phys. Rev. B **67**, 045413 (2003).
[19] R. Saito, C. Dresselhaus, and G. Dresselhaus, *Physical Properties of Carbon Nanotubes* (Imperial College Press, London, 1998), Chap. 7.
[20] G. D. Mahan, Phys. Rev. B **65**, 235402 (2002).
[21] M. S. Dresselhaus and P. C. Eklund, Adv. Phys. **49**, 705 (2000). Breathing mode for isolated single-wall nanotube is shown to be optical mode because the frequency $\omega \neq 0$ at $k=0$. The large value of V_T is reported in Fig. 14 caption.
[22] S. S. Savinskii and V. P. Peterovskii, Phys. Solid State **44**, 1802 (2002).
[23] H. Suzuura and T. Ando, Phys. Rev. B **65**, 235412 (2002).
[24] A. De Martino and R. Egger, Phys. Rev. B **67**, 235418 (2003). Breathing mode is considered as the TA mode even though they state the finite frequency at long wavelength.
[25] D. Sanchez-Portal, E. Artacho, J. M. Soler, A. Rubio, and P. Ordejon, Phys. Rev. B **59**, 12678 (1991). The TW mode speed decreases from 15.0 for (10,10) to 13.0 km/s in (4,4) nanotubes.